



Repair of Inconel 718 parts by Cold Spray Additive Manufacturing: The effect of substrate preheating on thick coatings properties

A. Garfias^a, P. Kindermann^b, R.F. Vaz^{a,c}, V. Albaladejo-Fuentes^{a,*}, J. Sánchez^a, I. Ünsal^b, G. Schlick^b, I.G. Cano^a

^a Thermal Spray Center (CPT), Universitat de Barcelona, Carrer de Martí i Franquès 1, Barcelona 08028, Spain

^b Fraunhofer IGCV, Am Technologiezentrum 10, Augsburg 86159, Germany

^c Center for Thermal Spray Research (CTSR), Stony Brook University, Room 130 Heavy Engineering Building, NY, USA

ARTICLE INFO

Keywords:

IN718
CSAM
Substrate preheating
Microstructure
Adhesion

ABSTRACT

Cold spray additive manufacturing (CSAM) has been developed as a promising solid-state technology for repair applications. Yet, one of the main challenges of CSAM is the deposition of high-strength materials, such as Inconel 718® (IN718), due to their low particle plasticity. IN718 is a high-performance Ni-based superalloy usually used in relevant applications such as high-temperature industries or jet engines. The interest in remanufacturing IN718 damaged parts with CSAM has increased in the last years; however, different deposition strategies still need to be studied to obtain well-bonded and dense IN718 deposits. This study investigates the effect of IN718 substrate preheating on the CSAM IN718 deposit microstructure and thickness, as well as the adhesion mechanisms and strength at room and preheating temperatures: 250 and 400 °C. The results revealed that a substrate preheating temperature of 400 °C promoted a dense microstructure within a 1.2 mm thick coating with porosity values < 0.1 %, and an adhesion strength > 50 MPa.

1. Introduction

Inconel 718 (IN718) is a high-performance Ni-based superalloy, registered by the US company *International Nickel Company*, with excellent corrosion resistance and high mechanical strength at high temperatures used in relevant applications, such as jet engines that operate at temperatures as high as 700 °C. Over the years, IN718 has been processed with conventional methods, i.e., wrought and cast techniques; however, its high strength characteristics make it difficult to machine using conventional processes [1,2]. Some IN718 parts are exposed to harsh environments, and their damages by erosion, abrasion, or hot corrosion may result in volume losses, which have been repaired by welding or other processes involving high-temperature deposition, resulting in microstructural effects on the IN718 base metal. Therefore, in the last years, cold spray additive manufacturing (CSAM) has been studied as an alternative for repairing IN718 damaged parts.

Cold spray (CS) is a solid-state deposition that has been developed for coatings and has advanced as an additive manufacturing (AM) technology with the potential to be used in repairing applications [3–6] In CS, a feedstock powder is injected inside a gun, and accelerated by a

preheated gas, typically N₂ or He, through a convergent-divergent de Laval nozzle, reaching supersonic velocities. The powder particles are accelerated and propelled towards a substrate (below the materials recrystallisation temperature); when they impact with enough kinetic energy, they deform plastically and remain adhered to the substrate, which are effectively explained in the references [7,8]. The speed which must be achieved for a material application, is called the critical velocity (v_{cr}). The most established theory on bonding mechanisms in CS is the work of Assadi et al. [9], where adiabatic shear instability (ASI) is proposed as the main adhesion mechanism responsible for the bonding of the particles. This phenomenon occurs due to the high strain rate deformation processes during the impact, which disrupt the superficial oxide film of the particles, creating a metal jet that forms a metallurgical bonding by establishing an intimate contact between the particles and the substrate. In addition to the ASI theory, Hussain et al. [10] studied the behavior of CS Cu particles on Al substrate, observing that the particles deform the substrate, creating a layer of particles mechanically interlocked, acting as a well-bonded base for further impacting particles to adhere.

Moreover, the CS deposition of high-strength materials, e.g., IN718,

* Corresponding author.

E-mail address: vicente.albaladejo@ub.edu (V. Albaladejo-Fuentes).

is still challenging; the lack of particle deformability at the impact hinders the bonding processes and may lead to a porous or low-adhesion deposit. Hence, the use of high-energy parameters is required to obtain dense deposits of IN718, which can result in an accumulation of residual stresses that may cause the detachment of the deposits from the substrate [11,12]. To overcome this, scholars have focused on different deposition strategies to obtain well bonded-dense CS IN718 deposits [11,13–18]. Singh et al. [16] measured the residual stress distribution in CS IN718 coatings with varying thicknesses, indicating that residual stresses significantly influence adhesion strength, which decreases by improving the coating thickness. Additionally, Sun et al. [15] studied the impact of surface roughness and substrate preheating on the coating-substrate bonding mechanism, revealing that a smoother substrate surface enhanced the plastic deformation of the particles without constraint. Moreover, the substrate preheating promoted metal jetting of the particles, resulting in higher bonding strength under shear loading. Pérez-Andrade et al. [11] optimized the CS process gas temperature conditions to produce thick IN718 coatings with low porosities, high hardnesses, and low tensile residual stresses in the substrate-coating interface. The authors also evaluated the effect of annealing and hot isostatic pressing (HIP) on the microstructure of the coatings. Annealing improves the deposit density, > 99 %. Ma et al. [14] compared the characteristics of CS IN718 produced with different propelling gases, He and N₂. Higher ductility and ultimate tensile strength were reported for IN718 coatings by using He instead of N₂. However, He increases CS repairing costs.

The interest in repairing IN718 parts with CSAM has grown in recent years [4–6]. However, studies on the CS process for IN718 are still limited. Consequently, various deposition strategies require further investigation to achieve well-bonded and dense IN718 thick deposits suitable for repairing applications. Substrate preheating has been shown to improve the adhesion strength when spraying hard materials due to the softening of the substrate, which allows the removal of the native oxide layer by ASI, resulting in an improved metallic bonding [19]. Ortiz-Fernandez et al. [19] showed an improvement of 30 % in the CS Al adhesion on Ti6Al4V substrate by its preheating by an induction system. Moreover, Ortiz-Fernandez and Jodoin [20] used an induction system for the Ti6Al4V substrate and the IN718 deposit, and an IN718 feedstock powder heater to control the temperatures of the materials during the deposition, promoting higher deposition efficiency (DE) and inter-particle bonding strength. Xie et al. [21] evaluated the bonding strength of CS 316 L stainless steel on a preheated 316 L substrate, resulting in adhesion of 13.4 MPa and 74.1 MPa at preheating temperatures of 25 and 700 °C, respectively.

Up to date, the impact of substrate preheating on IN718 coatings sprayed onto IN718 substrates has not been reported. This deposition strategy is an alternative for repairing damaged IN718 parts without detrimental effects on their material microstructures. This work investigates the influence of substrate preheating on CS IN718 thick deposits for repair applications. The variations in microstructural characteristics, including porosity, microhardness, and phase composition, of the deposits sprayed at different preheating temperatures (room temperature (RT), 250, and 400 °C) were evaluated. The interaction between the coating and the substrate at the different preheating temperatures was investigated, focused on the adhesion mechanisms of single impact splats. Furthermore, the bonding strength of the samples at varying thicknesses and preheating temperatures was tested to determine the effectiveness of the CS process for repairing IN718 parts.

2. Materials and methods

2.1. Feedstock powder

A commercial IN718 powder with dendritic microstructure (Diamalloy 1006, Oerlikon) was used in this study. Its particle shape and cross-section images were obtained by scanning electron microscopy

(SEM) in a Phenom ProX Desktop microscope, as seen in Fig. 1 (a-b). An elemental microanalysis was carried out with Quantax EDS Bruker Nano integrated into a SEM Jeol 5310 to measure the IN718 chemical composition, shown in Table I. The IN718 particle size distribution was analyzed with a laser diffraction particle sizing analyzer Beckman Coulter LS 13 320 via dry mode, presented in Fig. 1 (c).

2.2. CSAM parameters and preheating conditions

All samples were sprayed with a high-pressure CS Plasma Giken PCS 100 equipment on polished dia. 25 mm IN718 discs. To examine the impact of substrate preheating and thickness on the samples' microstructure and adhesion, the experiments detailed in Table II were conducted. The basis for the CS parameters used in this paper was previous internal research on CS parameter optimization of Inconel 718 based on obtaining the highest possible deposition efficiency. All samples were sprayed using the same CS parameters outlined in Table III.

The IN718 substrates were preheated using a hotplate CERAN 500; the hotplate's setpoint temperature was maintained during the spraying. The temperature of the substrates before spraying was measured using an infrared thermometer FLIR TG56.

To evaluate the adhesion mechanisms at the different preheating temperatures, single impact particle splats were sprayed with the CS parameters included in Tables II and III, with an adjusted traversal velocity of 1000 mm/s.

2.3. Microstructural characterization

The metallographic preparation of the samples was completed following the ASTM E1920–03 standard; the polished samples were etched in a reagent composed of 5 ml HF, 5 ml HNO₃, 5 ml H₂O₂, 10 ml HCl, and 5 ml distilled water to reveal their microstructure. Each samples' cross-sectional surface and thickness were evaluated with a Keyence VK-X series laser microscope according to the ASTM E3–11 standard. The mean porosity values were obtained using *ImageJ* software of images obtained by optical microscopy (OM) in a Leica DM5000 microscope, following the ASTM E2109–01 standard. The Vickers microhardness was obtained from a mean value of ten indents for each sample in accordance with ASTM E384–17 standard, with a 0.3 kgf (HV_{0.3}) using a Shimadzu HV-2/HMV-2T equipment.

To evaluate the composition of the deposits, an elemental mapping was obtained with EDS detector GATAN MONO-CL4 attached to a FESEM JEDL J-7100. To evaluate the phase changes, XRD patterns were performed for the feedstock powder and CS samples, using an equipment PANalytical X'Pert PRO MPD with Ni filtered K α radiation ($\lambda = 1.5418 \text{ \AA}$) from 5 to 100° 2 θ with a step size of 0.026° and measuring time of 100 s.

2.4. Adhesion mechanisms & evaluation

To investigate the adhesion mechanisms, the single impact splats were observed with a Phenom ProX Desktop SEM. The adhesion strength of the CS IN718 deposits with an IN718 substrate was evaluated with equipment Servosis ME 402–10, according to the ASTM C633–13 standard. The tensile specimens included a cylinder substrate fixture with the IN718 coating and a loading fixture counterpart; both of them with a 1 in. diameter and 1.5 in. in length. For each variable, three samples were glued to a grit-blasted counterpart with the adhesive HTK Ultra-bond 100 with a strength of 50 MPa; a tensile test at a rate of 0.01 mm/s was performed until failure according to the diagram included in Fig. 2. The fracture surfaces were observed in SEM to interpret the type of failure: adhesive (on the interface substrate-coating), cohesive (between the coating particles), or glue failure (in the interface coating-counterpart).

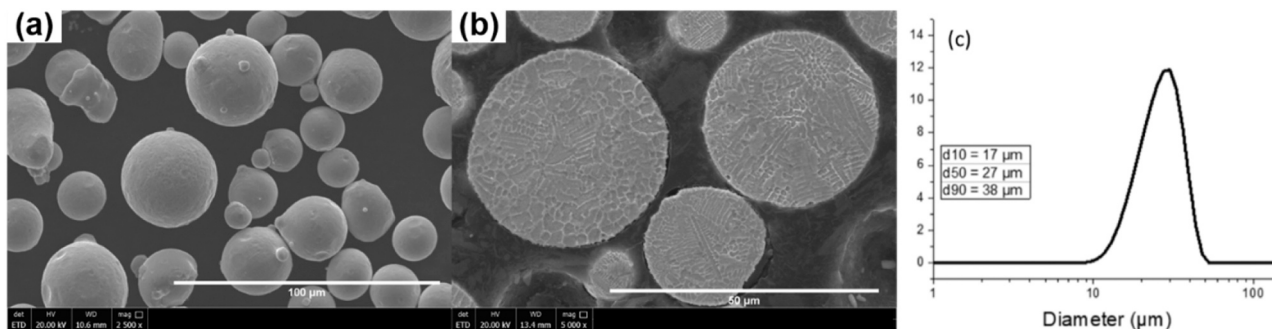


Fig. 1. Feedstock powder IN718 (a) particle shape, (b) cross-section microstructure, and (c) particle size distribution.

Table I

Feedstock powder IN718 chemical composition (wt%).

Ni	Cr	Fe	C	Nb	Mo	Al	Ti
49.17	19.06	17.33	4.69	4.69	3.02	1.05	0.99

Table II

CS samples nomenclature and characteristics.

Label	Preheating Temperature (°C)	Number of layers
RT-10	Room Temperature	10
RT-15		15
RT-20		20
RT-40		40
250-10	250	10
250-15		15
250-20		20
250-40		40
400-10	400	10
400-15		15
400-20		20
400-40		40

Table III

CS parameters.

Pressure (MPa)	Temperature (°C)	Standoff Distance (mm)	Traversal velocity (mm/s)
7.0	1080	30	500

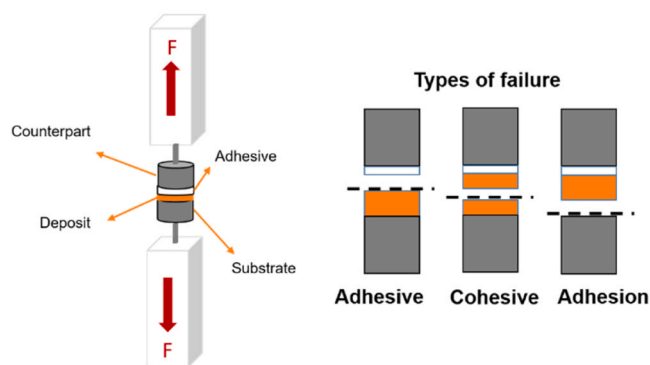


Fig. 2. Adhesion test setup and scheme of types of failure.

3. Results and discussion

3.1. Microstructural characterization

Fig. 3 shows the samples' cross-sectional microstructures, while the

porosity and microhardness are also presented in Fig. 4. Overall, dense and homogeneous CS IN718 deposits were obtained with no visible cracks nor delamination areas, which is consistent with other studies of CS IN718 in the literature [11,16,18]. Furthermore, all micrographs revealed a smooth substrate-deposit interface, indicating a strong bonding between particles and substrate, and an adequate selection of the CS parameters and substrate activation. In addition, the microstructural characteristics of the 40 layered deposits were similar to the ones sprayed with fewer layers; despite the higher thickness, a dense microstructure with a smooth interface without defects was observed.

As observed in Fig. 3, two effects that led to microstructure densification are clearly distinguishable: the temperature effect from the substrate preheating and the peening effect of the particles related to the increase in coating thickness. The effect of the substrate preheating on the microstructure densification of the samples was notable, especially on the first deposited layer, where the temperature transfer from the substrate was more influential. In this case, regardless of the number of layers sprayed, the samples exhibited higher porosity values when sprayed at RT compared to those sprayed with preheating temperatures of 250 and 400 °C. This effect was the most evident in the 20 layered samples; the porosity decreased with the preheating substrate temperature increase, resulting in porosity values of $2.2 \pm 0.8\%$, $1.2 \pm 0.4\%$, and $0.5 \pm 0.2\%$ for RT-20, 250-20, and 400-20, respectively. This is attributed to an enhanced plastic deformation of the particles when impacting a surface at a higher temperature, promoting metallurgical bonding and micro welding between particles-substrate and particles-particles [21]. Moreover, the peening effect from the subsequent impingent particles was also observed in the porosity. In all cases, the porosity decreased when increasing the deposits' thickness: resulting in values of $2.3 \pm 0.6\%$ and $1.5 \pm 0.5\%$ for samples RT-10 and RT-40, $1.0 \pm 0.3\%$ and $0.6 \pm 0.2\%$ for samples 250-10 and 250-40, and $1.2 \pm 0.7\%$ and $0.1 \pm 0.1\%$ for samples 400-10 and 400-40, respectively. In particular, as reported by Singh et al. [16] at higher thicknesses the peening effect is intensified, leading to a higher deformation of the already deposited particles by the impact of the subsequent particles, acting to reduce the previous deposited layers' thickness and densifying them.

In particular, sample 400-40 presented a fully dense microstructure (99.9%) comparable to an IN718 bulk part. It is worth noting that there are no reported CS IN718 deposits within the literature exhibiting such a highly dense microstructure. For instance, Singh et al. [16] studied the influence of deposit thickness (ranging from 216 to 1173 μm) on the residual stress development of CS IN718 deposits sprayed with N₂ onto IN718 substrates, obtaining deposits with low porosity values of $0.7 \pm 0.3\%$. However, discontinuous gaps between the particles-substrate for all thicknesses can be observed in the interface, suggesting a weak adhesion strength. Another example is the study of Ma et al. [14], in which the microstructures of CS IN718 deposits fabricated using N₂ and He were compared. The deposits sprayed with N₂ exhibited a dense microstructure, yet even after a heat treatment post-processing, the porosity resulted in a value of $1.24 \pm 0.14\%$. On the other hand, the

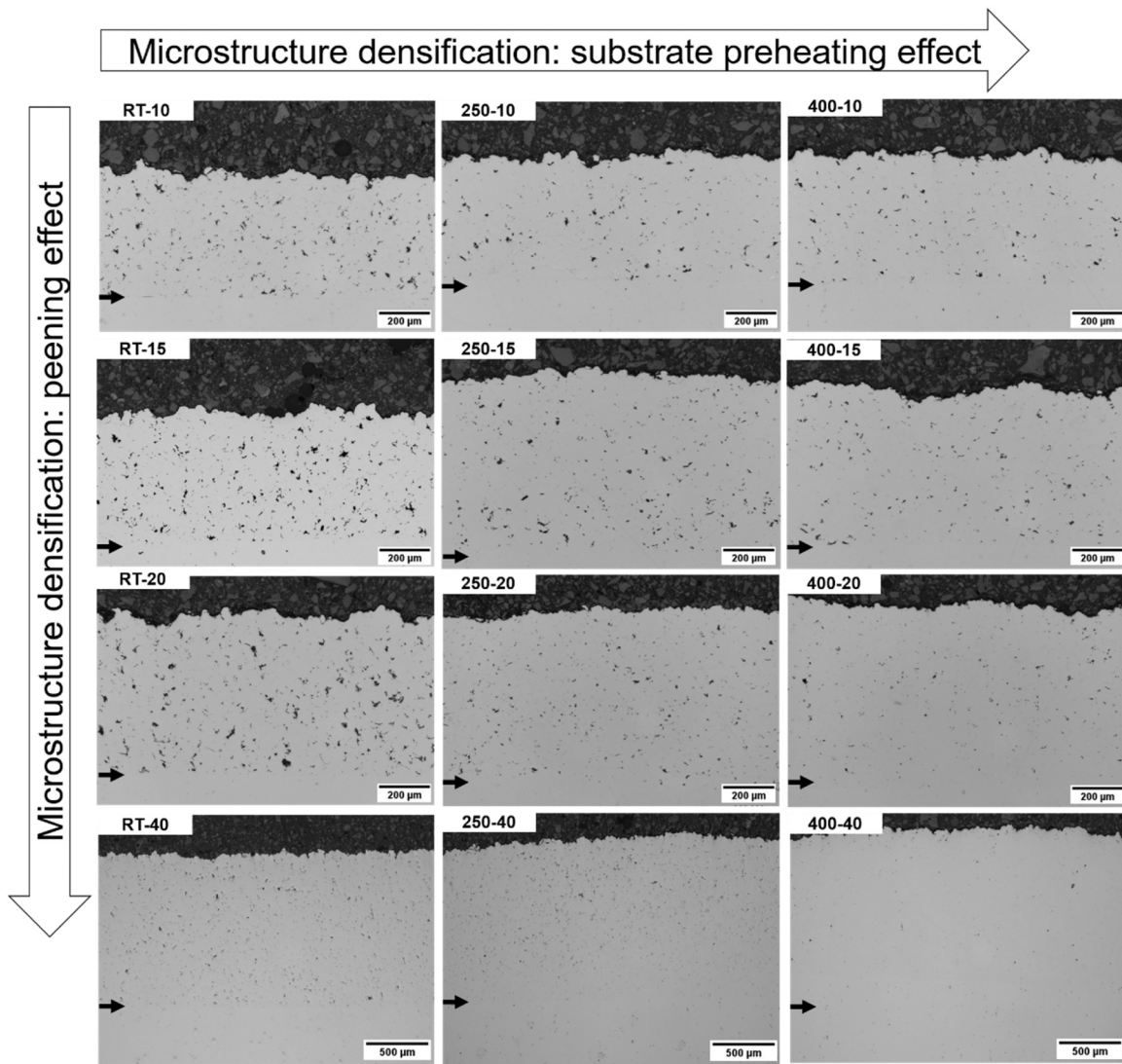


Fig. 3. OM images of the CS IN718 deposits. The arrows indicate the interface deposit-substrate.

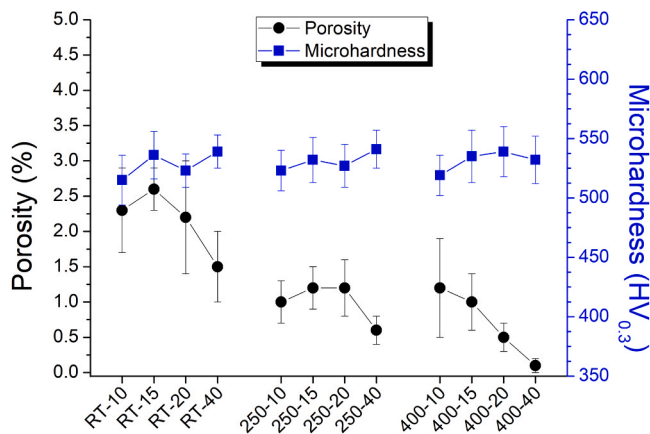


Fig. 4. Porosity and microhardness of CS IN718 deposits.

deposits obtained with He, showed a fully dense microstructure with porosity values of 0.21 ± 0.05 % in the as-sprayed state and 0.18 ± 0.04 % after the heat treatment. Nonetheless, using He severely increases the costs associated with the CS processing, making its utilization difficult to justify [22]. Finally, Pérez-Andrade et al. [11] produced

CS IN718 deposits with 1.3 mm thickness and investigated the effects of a three-step heat treatment post-processing, obtaining a thick as-sprayed deposits sprayed with optimized conditions with a porosity value of 1.3 ± 0.1 % and no debonding signs, as well as heat treated specimens with dense microstructures containing 0.3 ± 0.1 % porosity.

In terms of microhardness, all values were comparable among all the CS IN718 deposits. In contrast to the work of Singh et al. [16], no difference in the microhardness was observed by increasing the deposits' thickness since all the samples in this work presented a dense microstructure with a strong cohesion between particles. Moreover, all the obtained microhardness values resulted in higher than the ones reported in the literature for bulk IN718 ($450 \text{ HV}_{0.3}$) [16,23] due to the inherent cold-working effect of the particles in the CS process [24].

Moreover, Fig. 5 presents graphically the thickness evolution of the IN718 deposits with the substrate preheating and number of layers. As expected, the deposits' thickness varied with the number of CS layers. For all 10 layered samples, the deposits' thickness remained constant, independently of the preheating temperature, resulting in similar values of $495 \pm 23 \mu\text{m}$, $498 \pm 14 \mu\text{m}$, and $467 \pm 25 \mu\text{m}$, for RT-10, 250-10, and 400-10, respectively. Each of the ten layers had a thickness close to $50 \mu\text{m}$. In the case of the RT samples, as the total number of layers was increased, thinner individual layers were obtained with mean values of $35 \mu\text{m}/\text{layer}$, $34 \mu\text{m}/\text{layer}$, and $29 \mu\text{m}/\text{layer}$ for RT-15, RT-20, and RT-

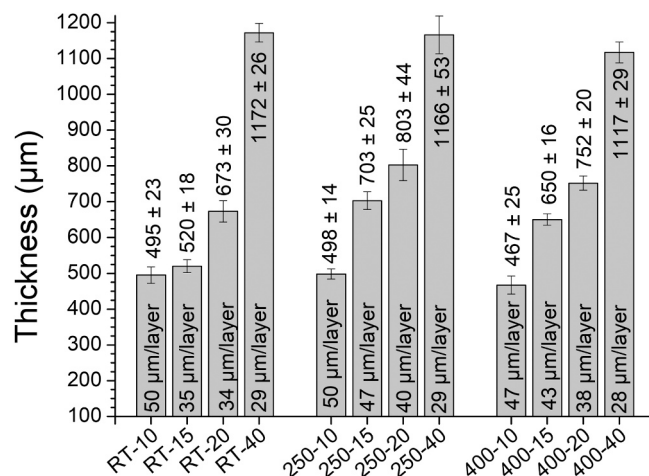


Fig. 5. Thickness of CS IN718 deposits.

40 samples, respectively. This tendency was less accentuated by controlling the substrate temperature, in which more than 40 $\mu\text{m}/\text{layer}$ were obtained until 20 layers for 250 and 400 $^{\circ}\text{C}$ preheating temperatures, which may be attributed to the temperature transfer resultant from both a higher substrate surface temperature and a higher temperature of the sample when spraying at longer times [12]. However, as the number of layers was increased to 40, the effect of the temperature was less influential in the deposit and a progressive decrease in the individual layers in all cases was observed regardless of the substrate temperature. This behavior is attributed to the fact that the CS process gas was sprayed at a higher temperature than the preheating temperatures, hence, after a prolonged spraying time the surface temperature of all samples eventually stabilized and no further differences in layers' thickness was observed. This steady-state temperature behavior is

consistent with the work of Legoux et al. [25] and Ortiz-Fernandez et al. [12], in which they recorded the temperature evolution of samples with and without preheating. In this sense, the measured thickness was similar for all preheating temperatures at 40 layers, with values of $1172 \pm 26 \mu\text{m}$, $1166 \pm 53 \mu\text{m}$, and $1117 \pm 29 \mu\text{m}$, for samples RT-40, 250-40, and 400-40, respectively.

Furthermore, the initial dendritic microstructure of the feedstock powder was maintained after the CS processing, as confirmed by the SEM micrograph and the EDS analysis shown in Fig. 6. The SEM image clearly shows the splats with the deformed dendritic microstructure localized in the periphery of the particles. In addition, the compactness of the particles was notably apparent since the particle boundaries were barely distinguished. The EDS element map distribution revealed a segregation of Nb, Mo, and C in the inter-dendritic regions, which showed that the microstructure of the powder was preserved during the CS process. The segregation of these elements in dendritic form is attributed to the rapid thermal changes, specifically to rapid solidification and large undercooling during the powder atomization process [26, 27].

One drawback of substrate preheating is that depending on the temperature and material involved, it may cause oxidation and hinder the bonding strength between the particles and the substrate [12,28]. Therefore, an XRD analysis was done to confirm the absence of oxides in the specimens at RT and 400 $^{\circ}\text{C}$, the highest preheating temperature. The diffractograms are shown in Fig. 7. There were no oxides present, and all the samples exhibited the same peaks, which correspond to the single-phase FCC solid solution (γ phase) of IN718 [26,29]. Typically, IN718 is a material known to form several phases and precipitates. In particular, the phases γ' and γ'' determine its mechanical characteristics. Even though these phases were not observed in the CS IN718 deposits, post-processing heat treatments can be applied to tailor the microstructure of the deposits, promoting the nucleation of the γ' and γ'' precipitates, while controlling other undesired phases [23].

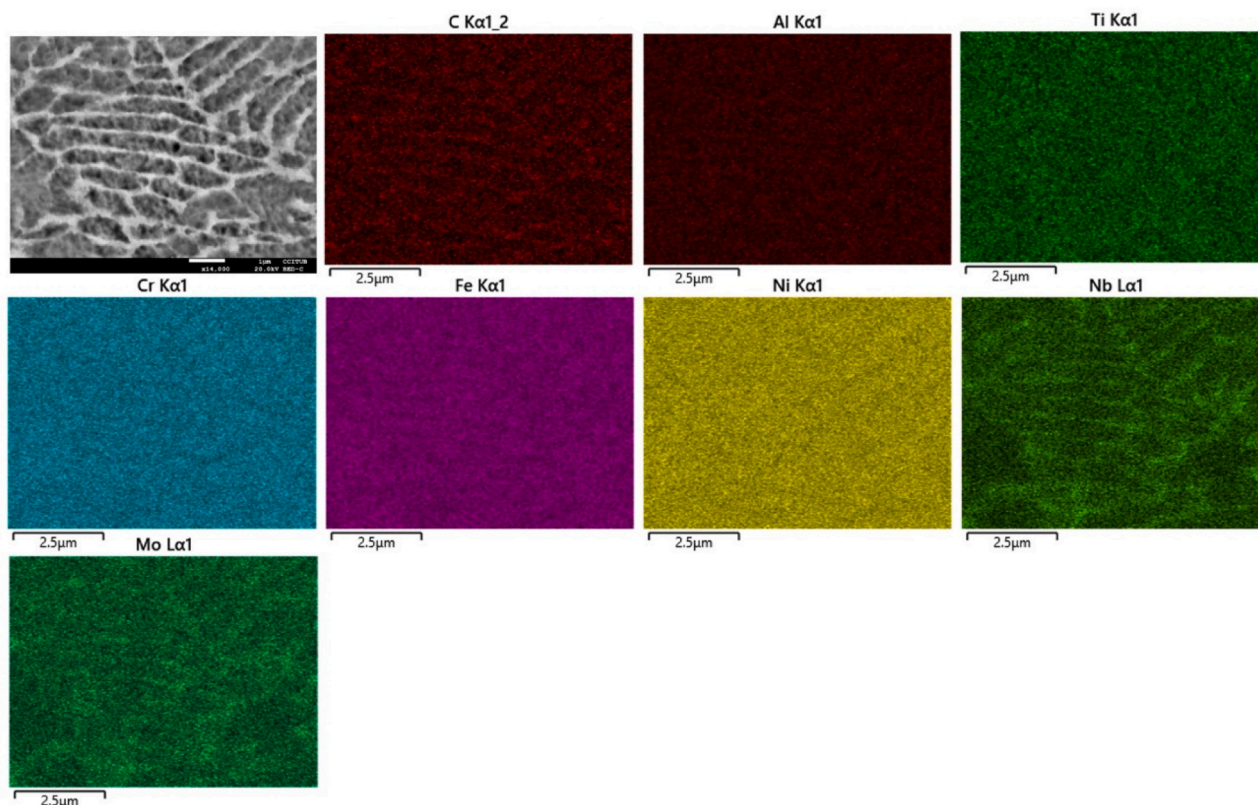


Fig. 6. EDS elemental map of the 400-40 deposit microstructure.

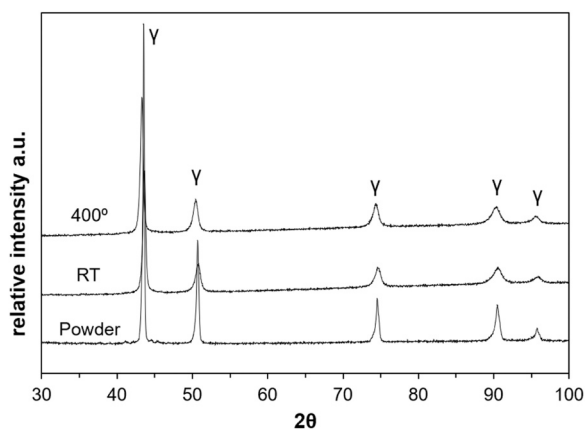


Fig. 7. XRD diffractograms of the IN718 feedstock powder, RT-40, and 400-40 deposits.

3.2. Adhesion mechanisms and strength

Dense IN718 coatings were obtained by selecting the optimized parameters for this material, in which the sprayed particles impacted the substrate at a velocity within the window of deposition, i.e., above the v_{cr} (between 787 and 830 m/s) and below the erosion velocity [13,14]. The fact that the substrate and the deposit were made from the same material influenced positively on both the particles' and the substrate plasticity at impact, which enhanced bonding due to their similar mechanical and microstructural properties; in general, the deposition of different materials still has been a challenge for CS processing because of the dissimilar material response at the impact, which can produce the erosion of the softer side and none deformation of the harder counterpart [19,30].

The two densification effects mentioned in the previous section, a higher substrate temperature and the peening effect of the particles at a high number of layers, facilitated the deformation and subsequent packing of the IN718 particles. Fig. 8 shows the OM images of the cross-sectional as-sprayed and etched microstructures of 40 layered IN718 deposits. As delineated by the dashed lines, the particles sprayed

without preheating temperature exhibited a slight deformation, while generally retaining a semi-spherical shape. In contrast, the deposits subjected to both preheating temperatures exhibited highly deformed particles, which facilitated a tighter packing that minimized inter-particle voids. This increased particle deformation with temperature is consistent with the findings of Ortiz-Fernandez et al. [12], which demonstrated that applying temperature to the specimen while spraying softens the deposit due to heat transfer processes. In this sense, the temperature transfer from the substrate to the deposit softened, up to a certain thickness, the already deposited particles, enhancing its deformation. When increasing the thickness beyond this point, the tampering effect of the particles becomes more influential, thereby densifying the microstructure [31].

To further investigate the interaction of the substrate at different temperatures and the particles, single splats were deposited by CS. Fig. 9 shows the SEM images of the sprayed particles and their cross-sectional microstructures. In neither case, the substrate exhibited any craters formed by the impact of bounced particles, which is attributed to the high-strength characteristics of the IN718 substrate. In addition, the particles in all cases were well attached and were plastically deformed with evidence of the metal jetting phenomenon [19,32,33]. In particular, the particles' cross-section showed this interaction with more detail; the particles sprayed onto the RT substrate only formed a slight jet, and their impact caused a slight deformation of the substrate. In this case, a gap at the center-bottom of the particles was present, which can be attributed this discontinuity in the interface to the higher temperature of the particles at the periphery than at the center, indicating that a lower temperature is reached in this center-bottom part of the particle, consequently hindering the bonding [15]. The same gap was observed in some of the particles sprayed onto the substrates preheated at 250 °C; however, for the substrates preheated at 400 °C, this void was almost nonexistent, indicating that the temperature of the substrate promoted adhesion [15,20,34,35]. To understand this phenomenon, the influence of temperature on the plastic deformation mechanisms of the particles must be considered. Upon impact, most kinetic energy from the particles is converted into heat. This increase in the local temperature facilitates the dislocation motion within the materials, increasing both substrate and particle deformation [36]. Consequently, localized melting occurs, which promotes the fracture of an oxide layer, thereby enhancing

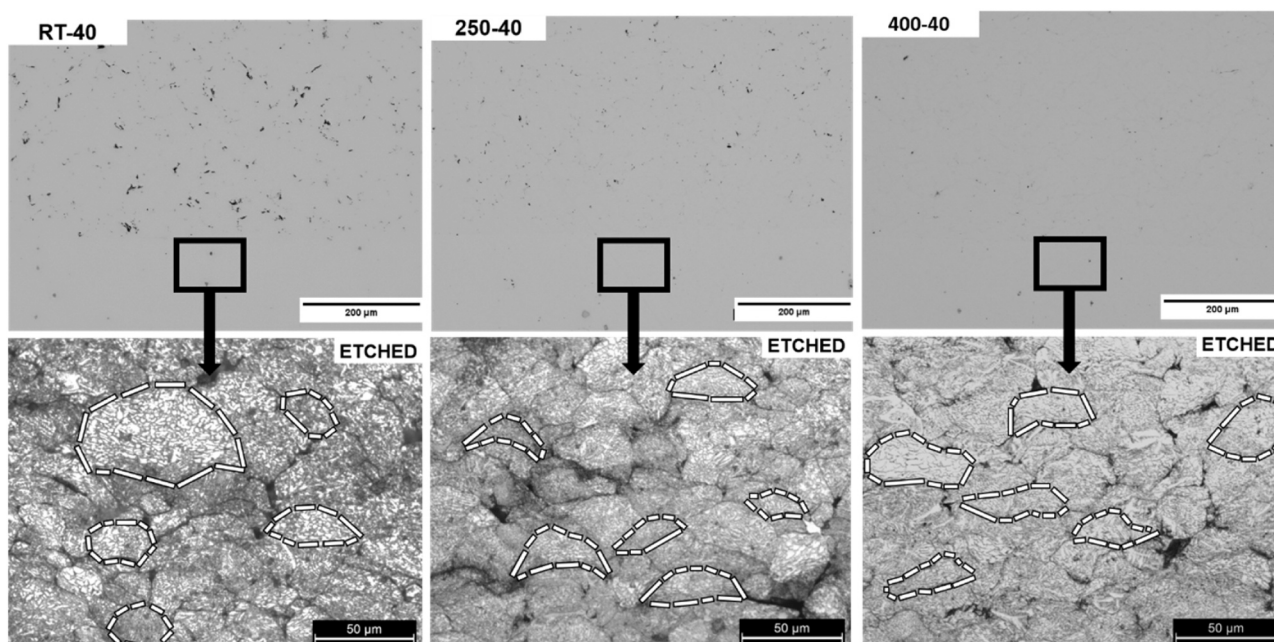


Fig. 8. OM images of the cross-sectional as-sprayed and etched 40 layered CS IN718 microstructures.

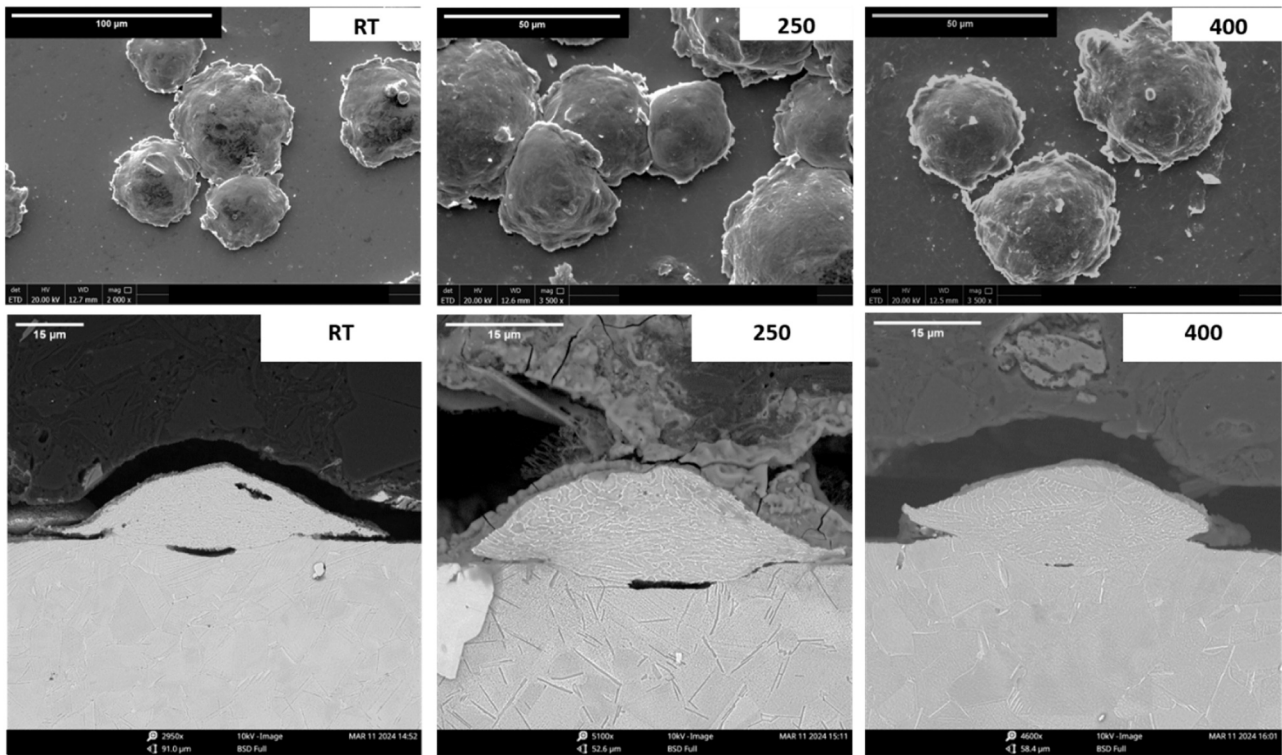


Fig. 9. SEM images of single splats of RT, 250, and 400 substrate preheating temperatures.

diffusion processes crucial for a successful adhesion between particles and substrate, and improved cohesion among particles [33,37]. Thus, an increased substrate or coating temperature induces a softening effect [20]. In the initial layers, this effect manifests as an enhanced metallurgical bonding at the interface, characterized by a strong intimate contact between the particles-substrate (Fig. 9). Subsequently, in the succeeding layers, this softening effect influences the already deposited particles, which subsequently undergo further deformation due to the peening effect. As a result, a densification in the microstructure and an increased adhesion strength are achieved.

The adhesion strength of the CS IN718 deposits on IN718 substrates is a critical requirement for ensuring adequate performance in repairing applications [5,38]. In general, the deposition of these high-strength materials remains challenging in the CSAM technology due to both a lack of particle deformability that hinders the bonding processes and the accumulation of residual stresses that promote the deposit detachment

[16,39]. Therefore, investigating of different deposition strategies, such as the robot path trajectory, substrate preheating, and optimization of the CS parameters are essential to ensure a strong bonding with the substrate [40]. Consequently, the effect of the substrate preheating on the adhesion of the CS IN718 deposits was investigated in this work; Fig. 10 shows the values obtained for CS IN718 deposits with different preheating conditions and layers.

In particular, the samples deposited without substrate preheating exhibited an adhesion strength with cohesive failure around 42 MPa. In contrast with the work of Singh et al. [16], in which the reported adhesion strength of 17 ± 3 MPa for CS IN718. The very close adhesion values for different RT coating thickness suggests that the accumulation of compressive residual stresses did not influence the cohesion nor adhesion of the CS IN718 deposits, which may be attributed to the quality of the deposits sprayed under optimized conditions.

Moreover, all samples subjected to substrate preheating exhibited

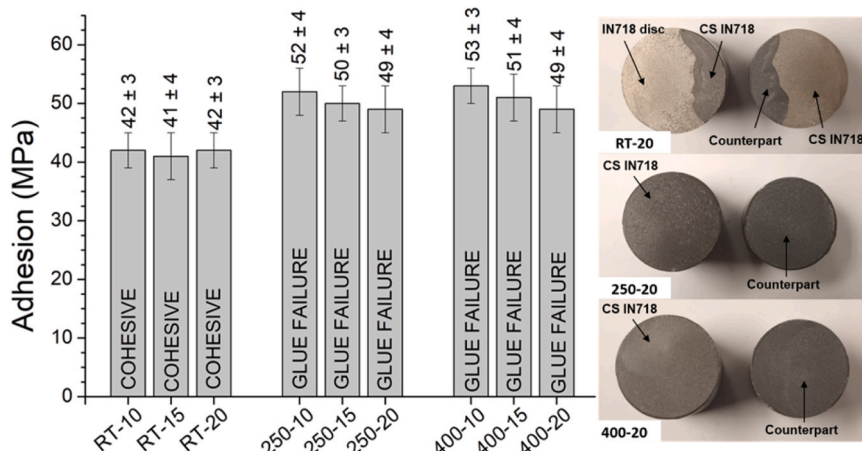


Fig. 10. Adhesion testing results of CS IN718 deposits.

glue failures, meaning that all these samples presented bonding strengths > 50 MPa, which indicated that the cohesion between particles and the adhesion to the IN718 substrate were greater than the RT specimens. Again, no adhesion variation with the different thicknesses was observed. The resulting adhesion strength of the deposits was notably restricted by the glue strength: 50 MPa, which is a strength coherent with the results seen in the literature, like the values presented by Shinde and Sampath [41] in a comparison between ASTM C633–12 and ISO 14916:2017 adhesion testing with different testing parameters, sample geometry, and glue manufacturers. For large deposits, like CSAM tens of millimeters thick, the literature presents some other adhesion techniques than the ASTM C633–13 testing for adhesion measuring. Vaz et al. [22] present a scheme for an ASTM E8–22 tensile testing adapted method, where the samples are machined and loaded to promote the failure in the deposit/substrate interface (adhesive mode) or in the deposit volume (cohesive mode), avoiding the glue failure. Ma et al. [14] show this scheme in detail for CSAM IN718 deposits. However, a bonding strength > 50 MPa would be suitable for general repair applications [42], avoiding new tests.

Furthermore, Fig. 10 shows representative images of the CS IN718 20 layered samples. It was evident from the images that the differences in failure were between the samples sprayed with and without substrate preheating. This trend persisted across all samples: the first presented glue failure, as the deposits remained attached to the IN718 substrate discs, while the counterparts were perfectly detached from the deposits. Whereas the second experienced cohesive failure as the deposit was delaminated, leaving some of it attached to the IN718 substrate discs and the remainder adhered to the counterpart. This suggests that the cohesion between samples was improved when applying higher temperatures to the substrate while spraying, consistent with the work of Sun et al. [43], which revealed that substrate preheating promoted metallurgical bonding and increased the deposit-substrate adhesion strength.

This enhancement of adhesion can be further investigated by observing the interface of the deposits, along with the characteristics of single impact splats and their interaction with the substrate. Fig. 11 presents the SEM micrographs of the etched interface of the RT-40, 250-40, and 400-40 CS IN718 deposits. The micrographs clearly showed a difference between the RT specimens and the preheated ones; the first one exhibited a discontinuous gap between the particles and the substrate surface, suggesting that only localized parts of the deformed particles were able to bond metallurgically due to the occurrence of ASI. Moreover, the particle layers were also notorious, as the particle boundaries were clearly visible, indicating a lack of cohesion between them. On the contrary, by preheating the substrate, the interfaces became highly smooth. Specimen 250-40 only showed some voids in the deposit-substrate interface, while sample 400-40 exhibited a continuous and dense interface. For these two deposits, the particles boundaries were barely distinguishable, which is consistent with the results observed in the single impact splats.

Overall, the substrate preheating strategy resulted in a significant

reduction of porosity within the microstructure of the CS IN718 deposits. Coatings exhibiting nearly fully dense microstructures (99.9 %) were manufactured without the presence of oxides or undesired phases, comparable to that of an IN718 bulk part. Moreover, thick deposits (> 1 mm) were successfully obtained with strong adhesion to the substrate and no signs of delamination.

These findings demonstrate significant potential for the implementation of CS in repairing applications that involve this alloy, and overcomes the challenge of processing IN718 fabricated by other methods, such as welding. In this context, potential limitations in industrial settings using this method may arise. For example, the setup for the preheating of large or complex damaged parts using a hotplate can be challenging. This limitation may need exploring alternative preheating methods that ensure a uniform temperature distribution on the damaged surface, such as induction heating [12]. In addition, ensuring an efficient surface preparation of the damaged part prior to deposition is crucial, which would require the development of a standardized polishing procedure. Furthermore, in high-performance sectors like the aerospace industry, repaired components must meet stringent requirements. Thus, the properties of the repaired parts would need to be thoroughly evaluated to ensure compliance with industry standards.

These limitations lay the groundwork for future research related to this work, focusing on the near-net-shape CS repair or reconstruction of the IN718 damaged components (i.e. turbine blades) through the implementation of novel toolpath trajectories. Additionally, evaluating the long-term performance of the refurbished parts under specific service conditions is essential for their successful application in industrial settings.

4. Conclusions

In this work, CS IN718 deposits on IN718 substrate were manufactured under different substrate preheating temperatures: RT, 250, and 400 °C. After the characterization and evaluation of the deposits regarding their microstructure, adhesion, and bonding mechanisms, the following conclusions can be drawn based on the results:

- CS processing can be successfully applied for repairing IN718 damaged parts by depositing the same material without adding any bond coating or other additional pre-processing other than polishing and cleaning, preserving the feedstock material microstructure and phase composition;
- Two effects led to microstructure densification: the temperature effect induced by the substrate preheating in the first layers, and the peening effect of the particles in the subsequent layers;
- The substrate preheating improved the bonding strength, adhesion, and cohesion of CS IN718 deposits by softening the substrate, which improved the materials' plasticity;
- The substrate preheating and deposit thickness did not affect the deposit microhardness; however, increasing the preheating

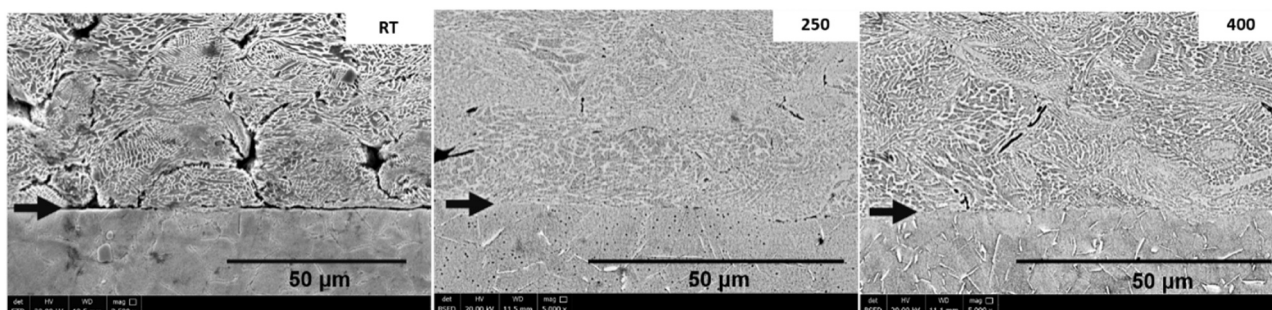


Fig. 11. SEM images of the etched substrate-deposit interface of the RT-40, 250-40, and 400-40 deposits. The arrows indicate the interface deposit-substrate.

temperature and the deposit thickness improved the deposit density, reaching values comparable to an IN718 bulk reference, > 99.9 %.

CRediT authorship contribution statement

Vicente Albaladejo-Fuentes: Writing – original draft, Supervision, Methodology, Formal analysis, Conceptualization. **J. Sánchez:** Writing – review & editing, Validation, Supervision, Resources, Methodology, Conceptualization. **I. Ünsal:** Writing – review & editing, Supervision, Software, Resources, Project administration. **G. Schlick:** Writing – review & editing, Validation, Supervision, Software, Resources, Funding acquisition. **P. Kindermann:** Writing – original draft, Methodology, Investigation, Formal analysis, Data curation. **R.F. Vaz:** Writing – review & editing, Methodology, Formal analysis. **A. Garfias:** Writing – original draft, Methodology, Investigation, Formal analysis, Data curation, Conceptualization. **I.G. Cano:** Supervision, Project administration, Funding acquisition.

Declaration of Competing Interest

The authors declare that they have no known competing financial interests or personal relationships that could have appeared to influence the work reported in this paper.

Acknowledgements

Grant PID2020-115508RB-C21 funded by MICIU/AEI/ 10.13039/501100011033 and, as appropriate, by “ERDF A way of making Europe”, by the “European Union” or by the “European Union NextGenerationEU/PRTR” *Author* would like to thank AGAUR for grant 2021 FISDU 00300 and the University for the 2023 Doctoral International Stays Grant. *Author* is a Serra Hunter Fellow. *Institute* wants to express gratitude to the Freistaat Bayern and its Bavarian Ministry of Economic Affairs, Energy and Technology for the funding of this work, within the project MultiMat Bavaria II. The results in this paper were achieved within the scope of the research project ACCURACY (Grant No. RvS-SG20-3451-1/41/5).

Data availability

Data will be made available on request.

References

- [1] B. Izquierdo, S. Plaza, J.A. Sánchez, I. Pombo, N. Ortega, Numerical prediction of heat affected layer in the EDM of aeronautical alloys, *Appl. Surf. Sci.* 259 (2012) 780–790, <https://doi.org/10.1016/j.apsusc.2012.07.124>.
- [2] Q. Jia, D. Gu, Selective laser melting additive manufacturing of Inconel 718 superalloy parts: densification, microstructure and properties, *J. Alloy. Compd.* 585 (2014) 713–721, <https://doi.org/10.1016/j.jallcom.2013.09.171>.
- [3] W. Li, K. Yang, S. Yin, X. Yang, Y. Xu, R. Lupoi, Solid-state additive manufacturing and repairing by cold spraying: a review, *J. Mater. Sci. Technol.* 34 (2018) 440–457, <https://doi.org/10.1016/j.jmst.2017.09.015>.
- [4] Saboori A., Biamino S., Di Torino P., Gitardi D., Lombardi M. The Capacity of Cold Spray Additive Manufacturing Technology for Metallic Part Repairing. Euro PM2018, Bilbao: 2018.
- [5] S. Yin, P. Cavaliere, B. Aldwell, R. Jenkins, H. Liao, W. Li, et al., Cold spray additive manufacturing and repair: fundamentals and applications, *Addit. Manuf.* 21 (2018) 628–650, <https://doi.org/10.1016/j.addma.2018.04.017>.
- [6] C.A. Widener, O.C. Ozdemir, M. Carter, Structural repair using cold spray technology for enhanced sustainability of high value assets, in: *Procedia Manuf.* 21, Elsevier B.V, 2018, pp. 361–368, <https://doi.org/10.1016/j.promfg.2018.02.132>.
- [7] X. Yang, T. Meng, Y. Su, X. Chai, Z. Guo, S. Yin, et al., Evolution of microstructure and mechanical properties of cold spray additive manufactured aluminum deposit on copper substrate, *Mater. Sci. Eng. A* 891 (2024), <https://doi.org/10.1016/j.msea.2023.146024>.
- [8] X. Yang, H. Xu, Y. Su, T. Meng, X. Chai, Z. Guo, et al., Effect of continuous and random multi-particle impaction on the aluminum coating and copper substrate in cold spraying, *J. Mater. Res. Technol.* 33 (2024) 287–297, <https://doi.org/10.1016/j.jmrt.2024.09.056>.
- [9] H. Assadi, H. Kreye, F. Gärtner, T. Klassen, Cold spraying – A materials perspective, *Acta Mater.* 116 (2016) 382–407, <https://doi.org/10.1016/j.actamat.2016.06.034>.
- [10] T. Hussain, D.G. McCartney, P.H. Shipway, D. Zhang, Bonding mechanisms in cold spraying: the contributions of metallurgical and mechanical components, *J. Therm. Spray. Technol.* 18 (2009) 364–379, <https://doi.org/10.1007/s11666-009-9298-1>.
- [11] L.I. Pérez-Andrade, F. Gärtner, M. Villa-Vidaller, T. Klassen, J. Muñoz-Saldaña, J. M. Alvarado-Orozco, Optimization of Inconel 718 thick deposits by cold spray processing and annealing, *Surf. Coat. Technol.* 378 (2019), <https://doi.org/10.1016/j.surfcoat.2019.124997>.
- [12] R. Ortiz-Fernandez, B. Jodoin, Hybrid additive manufacturing technology: induction heating cold spray—part I: fundamentals of deposition process, *J. Therm. Spray. Technol.* 29 (2020) 684–699, <https://doi.org/10.1007/s11666-020-01005-w>.
- [13] W. Wong, E. Irissou, P. Vo, M. Sone, F. Bernier, J.G. Legoux, et al., Cold spray forming of Inconel 718, *J. Therm. Spray. Technol.* 22 (2013) 413–421, <https://doi.org/10.1007/s11666-012-9827-1>.
- [14] W. Ma, Y. Xie, C. Chen, H. Fukunuma, J. Wang, Z. Ren, et al., Microstructural and mechanical properties of high-performance Inconel 718 alloy by cold spraying, *J. Alloy. Compd.* 792 (2019) 456–467, <https://doi.org/10.1016/j.jallcom.2019.04.045>.
- [15] W. Sun, A.W.Y. Tan, A. Bhowmik, I. Marinescu, X. Song, W. Zhai, et al., Deposition characteristics of cold sprayed Inconel 718 particles on Inconel 718 substrates with different surface conditions, *Mater. Sci. Eng. A* 720 (2018) 75–84, <https://doi.org/10.1016/j.msea.2018.02.059>.
- [16] R. Singh, S. Schrufer, S. Wilson, J. Gibmeier, R. Vassen, Influence of coating thickness on residual stress and adhesion-strength of cold-sprayed Inconel 718 coatings, *Surf. Coat. Technol.* 350 (2018) 64–73, <https://doi.org/10.1016/j.surfcoat.2018.06.080>.
- [17] R. Singh, K.H. Rauwald, E. Wessel, G. Mauer, S. Schrufer, A. Barth, et al., Effects of substrate roughness and spray-angle on deposition behavior of cold-sprayed Inconel 718, *Surf. Coat. Technol.* 319 (2017) 249–259, <https://doi.org/10.1016/j.surfcoat.2017.03.072>.
- [18] S. Bagherifard, G. Roscioli, M.V. Zuccoli, M. Hadi, G. D’Elia, A.G. Demir, et al., Cold Spray Deposition of freestanding inconel samples and comparative analysis with selective laser melting, *J. Therm. Spray. Technol.* 26 (2017) 1517–1526, <https://doi.org/10.1007/s11666-017-0572-3>.
- [19] R. Ortiz-Fernandez, S. Imbriglio, R. Chromik, B. Jodoin, The role of substrate preheating on the adhesion strength of cold-sprayed soft particles on hard substrates, *J. Therm. Spray. Technol.* 30 (2021) 655–667, <https://doi.org/10.1007/s11666-020-01148-w>.
- [20] R. Ortiz-Fernandez, B. Jodoin, Toward efficient cold spraying of inconel 718: understanding the influence of coating and particle impact temperatures, *J. Therm. Spray. Technol.* 32 (2023) 188–207, <https://doi.org/10.1007/s11666-022-01490-1>.
- [21] Y. Xie, M.P. Planche, R. Raelison, H. Liao, X. Suo, P. Hervé, Effect of substrate preheating on adhesive strength of SS 316L cold spray coatings, *J. Therm. Spray. Technol.* 25 (2016) 123–130, <https://doi.org/10.1007/s11666-015-0312-5>.
- [22] R.F. Vaz, A. Garfias, V. Albaladejo, J. Sanchez, I.G. Cano, A review of advances in cold spray additive manufacturing, *Coatings* 13 (2023), <https://doi.org/10.3390/coatings13020267>.
- [23] J.C. Franco-Correa, E. Martínez-Franco, J.M. Alvarado-Orozco, L.A. Cáceres-Díaz, D.G. Espinosa-Arbelaez, J.A. Villada, Effect of conventional heat treatments on the microstructure and microhardness of IN718 obtained by wrought and additive manufacturing, *J. Mater. Eng. Perform.* 30 (2021) 7035–7045, <https://doi.org/10.1007/s11665-021-06138-9>.
- [24] M.R. Rokni, S.R. Nutt, C.A. Widener, V.K. Champagne, R.H. Hrabec, Review of relationship between particle deformation, coating microstructure, and properties in high-pressure cold spray, *J. Therm. Spray. Technol.* 26 (2017) 1308–1355, <https://doi.org/10.1007/s11666-017-0575-0>.
- [25] J.G. Legoux, E. Irissou, C. Moreau, Effect of substrate temperature on the formation mechanism of cold-sprayed aluminum, zinc and tin coatings, *J. Therm. Spray. Technol.* 16 (2007) 619–626, <https://doi.org/10.1007/s11666-007-9091-y>.
- [26] A. Balasundaram, A. Bisht, M. Anantharaman, S.R. Bakshi, M. Kamaraj, Effect of double-aging heat treatment on microstructure and tribological behaviour of cold sprayed IN718 coating, *Met. Mater. Int.* 30 (2024) 483–500, <https://doi.org/10.1007/s12540-023-01507-6>.
- [27] X. Li, J.J. Shi, C.H. Wang, G.H. Cao, A.M. Russell, Z.J. Zhou, et al., Effect of heat treatment on microstructure evolution of Inconel 718 alloy fabricated by selective laser melting, *J. Alloy. Compd.* 764 (2018) 639–649, <https://doi.org/10.1016/j.jallcom.2018.06.112>.
- [28] X.K. Suo, M. Yu, W.Y. Li, M.P. Planche, H.L. Liao, Effect of substrate preheating on bonding strength of cold-sprayed Mg coatings, *J. Therm. Spray. Technol.* 21 (2012) 1091–1098, <https://doi.org/10.1007/s11666-012-9803-9>.
- [29] A.M. Ralls, M. Daroonparvar, M. John, S. Sikdar, P.L. Menezes, Solid-state cold spray additive manufacturing of ni-based superalloys: processing–microstructure–property relationships, *Materials* 16 (2023), <https://doi.org/10.3390/ma16072765>.
- [30] A. Bruera, P. Puddu, S. Theimer, M. Villa-Vidaller, A. List, G. Bolelli, et al., Adhesion of cold sprayed soft coatings: effect of substrate roughness and hardness, *Surf. Coat. Technol.* 466 (2023), <https://doi.org/10.1016/j.surfcoat.2023.129651>.
- [31] W. Li, C. Cao, S. Yin, Solid-state cold spraying of Ti and its alloys: a literature review, *Prog. Mater. Sci.* 110 (2020), <https://doi.org/10.1016/j.pmatsci.2019.100633>.
- [32] H. Assadi, F. Gärtner, T. Stoltenhoff, H. Kreye, Bonding mechanism in cold gas spraying, *Acta Mater.* 51 (2003) 4379–4394, [https://doi.org/10.1016/S1359-6454\(03\)00274-X](https://doi.org/10.1016/S1359-6454(03)00274-X).

- [33] A. Nastic, B. Jodoin, D. Poirier, J.G. Legoux, Particle temperature effect in cold spray: a study of soft particle deposition on hard substrate, *Surf. Coat. Technol.* 406 (2021), <https://doi.org/10.1016/j.surfcoat.2020.126735>.
- [34] Y. Watanabe, C. Yoshida, K. Atsumi, M. Yamada, M. Fukumoto, Influence of substrate temperature on adhesion strength of cold-sprayed coatings, *J. Therm. Spray. Technol.* 24 (2014) 86–91, <https://doi.org/10.1007/s11666-014-0165-3>.
- [35] C.W. Ziemian, M.M. Sharma, B.D. Bouffard, T. Nissley, T.J. Eden, Effect of substrate surface roughening and cold spray coating on the fatigue life of AA2024 specimens, *Mater. Des.* 54 (2014) 212–221, <https://doi.org/10.1016/j.matdes.2013.08.061>.
- [36] J. Vlcek, L. Gimeno, H. Huber, E. Lugscheider, A systematic approach to material eligibility for the cold-spray process, *J. Therm. Spray. Technol.* 14 (2005) 125–133, <https://doi.org/10.1361/10599630522738>.
- [37] G. Bae, Y. Xiong, S. Kumar, K. Kang, C. Lee, General aspects of interface bonding in kinetic sprayed coatings, *Acta Mater.* 56 (2008) 4858–4868, <https://doi.org/10.1016/j.actamat.2008.06.003>.
- [38] Ogawa K., Seo D. Repair of Turbine Blades Using Cold Spray Technique. *InTechOpen*; 2011. <https://doi.org/10.5772/664>.
- [39] V. Luzin, K. Spencer, M.X. Zhang, Residual stress and thermo-mechanical properties of cold spray metal coatings, *Acta Mater.* 59 (2011) 1259–1270, <https://doi.org/10.1016/j.actamat.2010.10.058>.
- [40] W. Li, C. Cao, G. Wang, F. Wang, Y. Xu, X. Yang, Cold spray + ' as a new hybrid additive manufacturing technology: a literature review, *Sci. Technol. Weld. Join.* 24 (2019) 420–445, <https://doi.org/10.1080/13621718.2019.1603851>.
- [41] S. Shinde, S. Sampath, A critical analysis of the tensile adhesion test for thermally sprayed coatings, *J. Therm. Spray. Technol.* 31 (2022) 2247–2279, <https://doi.org/10.1007/s11666-022-01468-z>.
- [42] X. Luo, G.M. Smith, S. Sampath, On the interplay between adhesion strength and tensile properties of thermal spray coated laminates—part i: high velocity thermal spray coatings, *J. Therm. Spray. Technol.* 27 (2018) 296–307, <https://doi.org/10.1007/s11666-018-0695-1>.
- [43] W. Sun, A. Bhowmik, A.W.Y. Tan, R. Li, F. Xue, I. Marinescu, et al., Improving microstructural and mechanical characteristics of cold-sprayed Inconel 718 deposits via local induction heat treatment, *J. Alloy. Compd.* 797 (2019) 1268–1279, <https://doi.org/10.1016/j.jallcom.2019.05.099>.